Inorganic Chemistry

Article

Cite This: Inorg. Chem. 2018, 57, 13486−13493

pubs.acs.org/IC

Ligand-Assisted Metal-Centered Electrocatalytic Hydrogen Evolution upon Reduction of a Bis(thiosemicarbazonato)Ni(II) Complex

Rahul Jain,[†] Abdullah Al Mamun,[†] Robert M. Buchanan,[†] Pawel M. Kozlowski,[†,‡] and Craig A. Grapperhaus*[,†]

[†]Department of Chemistry, University of Louisville, 2320 South Brook Street, Louisville, Kentucky 40292, United States

[‡]Department of Food Sciences, Medical University of Gdansk, Al. Gen. J. Hallera 107, 80-416 Gdansk, Poland

Supporting Information

ABSTRACT: In this study, we report the electrocatalytic behavior of the neutral, monomeric Ni(II) complex of diacetyl-bis(*N*-4-methyl-3-thiosemicarbazonato), NiL^1, for ligand-assisted metal-centered hydrogen evolution in acetonitrile (ACN) and dimethylformamide (DMF). Using foot-of-the-wave analysis (FOWA), NiL^1 displays a maximum turnover frequency (TOF) of 4200 and 1200 s^{-1} for acetic acid (CH_3COOH) in ACN and DMF, whereas for trifluoroacetic acid (CF_3COOH) the TOFs are 1300 and 120 s^{-1} in ACN and DMF, respectively. In ACN, the overpotentials are 0.53 and 0.67 V for CH_3COOH and CF_3COOH, respectively. In DMF, the overpotential is 0.85 V for CH_3COOH. First-order dependence with respect to the catalyst is established. NiL^1 displays a minimum Faradaic efficiency of 87% from controlled potential electrolysis. Gas analysis from controlled potential electrolysis in both ACN and DMF using CH_3COOH and CF_3COOH confirms NiL^1 as an electrocatalyst to produce H_2. In ACN, TONs of 48 and 24 were obtained for CH_3COOH and CF_3COOH, respectively in 4 h. In DMF, TONs of 13 and 3 were obtained for CH_3COOH and CF_3COOH, respectively. The H_2 evolution reaction was evaluated using deuterated acid, demonstrating an inverse kinetic isotope, which is consistent with formation of a metal hydride intermediate. A proposed ligand-assisted metal-centered mechanism for HER is supported by computational investigations. All catalytic intermediates in the proposed mechanism were structurally and energetically characterized using density functional theory (DFT), with the B3LYP/6-311g(d,p) and BP86/TZV/P in solution modeled via polarizable continuum model. The final step of catalysis involves the reaction of $[HNi(L^1\cdot)]^-$ with H^+ generating H_2. The correctness of proposed mechanism was confirmed by location of corresponding transition state (TS) having single imaginary frequency (i1786 cm^{-1}).

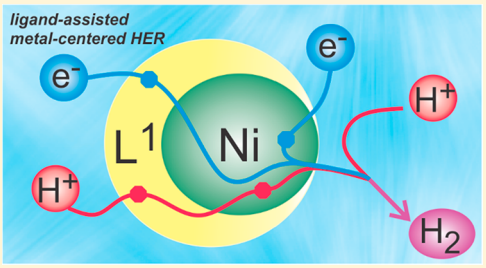

INTRODUCTION

In the pursuit of carbon-free fuels, hydrogen can be considered as an apt energy carrier.[1,2] Molecular hydrogen is generated by the two-electron reduction of protons through the hydrogen evolution reaction (HER).[3−5] The stored energy can be extracted on demand via the hydrogen oxidation reaction (HOR).[6] To date, Pt serves as an excellent electrocatalyst to generate hydrogen, but its high cost and limited availability has inspired the search for economically viable, earth abundant catalysts.[7−11] Typically, HER catalysts operate via a metal-centered route involving a metal hydride.[12−18] However, recently, a number of HER catalysts have been reported following alternate, ligand-centered pathways.[19−27]

Bis(thiosemicarbazone) complexes are a class of Schiff base systems possessing a tetradentate, square planar N_2S_2 coordination sphere that have received recent attention as HER catalysts.[28,29] The ligands are considered redox non-innocent as the terminal α-diimine unit is subject to reduction yielding a π-radical anion.[30−33] The soft donor ligand architecture stabilizes first-row transition metal ions in low oxidation states.[30,34−38] The first reported bis-(thiosemicarbazone) complex as a HER catalyst was the neutral monomeric zinc complex, ZnL^1, [L^1 = diacetyl-bis(*N*-4-methyl-3-thiosemicarbazonato)], which evolves hydrogen via a dinuclear, ligand-centered reaction.[23] The copper complex, CuL^1, catalyzes HER via a metal-assisted ligand-centered process in which H_2 is evolved at the ligand-center with the metal serving as an electron reservoir.[22] Straistari et al. reported a monomeric nickel complex, NiL^2, (L^2 = 4-{bis[4-(*p*-methoxyphenyl)-thiosemicarbazonato]}-2,3-butane) that also catalyzes HER.[39] NiL^2 was proposed to operate via a ligand-assisted metal-centered route in which Ni(III)-H was suggested as the catalytically active species. In this study, we report the HER activity of NiL^1 using CH_3COOH and CF_3COOH as external proton sources in ACN and DMF solutions. Mechanistic details have been investigated experimentally and computationally by employing density functional theory calculations in both gas phase and solution phase modeled via the polarizable continuum model (PCM). The

Received: July 25, 2018
Published: October 12, 2018

DOI: 10.1021/acs.inorgchem.8b02110
Inorg. Chem. 2018, 57, 13486−13493

results support a ligand-assisted metal-centered pathway (Scheme 1) and provide evidence to support the prior suggestion of Ni(III)-H as an intermediate for HER.

Scheme 1. Overview of First-Row Transition Metals with Bis(thiosemicarbazone) Ligands

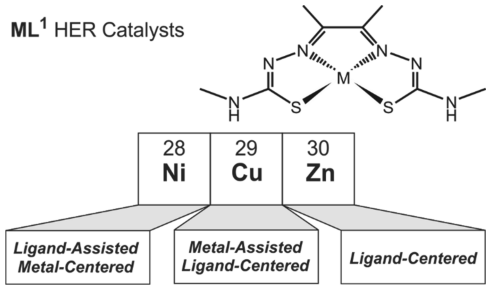

EXPERIMENTAL SECTION

Materials and Reagents. Chemicals, reagent-grade, were purchased from commercial sources and used without further purification unless otherwise noted. ACN and DMF solvents were dried using an MBraun solvent purification system. The nickel complex of diacetyl-bis(*N*-4-methyl-3-thiosemicarbazonato), NiL^1, was prepared as previously reported by West.[40]

Electrochemical Methods. A Gamry Interface potentiostat/galvanostat was used to record all cyclic voltammetry (CV) and controlled potential coulometry (CPC) measurements. Overpotential for hydrogen evolution was calculated using the methods reported by Fourmond et al. from the theoretical half wave potential, $E^{T}_{1/2,}$ and the experimental potential $E_{cat/2,}$ eq 1.[41] The value of $E_{cat/2}$ is defined as the potential required to obtain $i_{cat/2}$, one-half of the maximum of catalytic current. The turnover frequency (TOF) for hydrogen evolution was estimated using the foot-of-the-wave analysis (FOWA).[42−45] Sample calculations of overpotential and TOF are included in the Supporting Information.

$$\text{Overpotential } (\eta) = |E^{T}_{1/2} - E_{cat/2}| \quad (1)$$

The CV data were collected using a three-electrode cell comprised of a glassy carbon working electrode, platinum wire counter electrode, and Ag/Ag^+ reference electrode. The glassy carbon working electrode was polished using an aqueous alumina slurry before recording the data. The working and counter electrodes were washed with water, ethanol, isopropanol, acetone, ACN, and DMF before use. After the washing, the electrodes were sonicated for 10 min in the working solvent (ACN or DMF). The three-necked electrochemical cell used for CV studies was washed and dried in an oven overnight before use. In a typical CV experiment, a 0.30 mM solution of the catalyst was prepared in the working solvent (ACN or DMF) containing 0.1 M tetrabutylammonium hexafluorophosphate (TBAHFP) as supporting electrolyte. The solution was sparged with nitrogen for ∼15 min and then kept under a nitrogen atmosphere. Data were collected at scan rates of 0.2, 0.5, and 1.0 V/s. An aliquot of acid was added, and CV data were collected at all three scan rates. The next aliquot was not added until constant current was obtained at each scan rate. Additions of acid were continued until the current saturated. Under acid saturating conditions, the scan rate was varied until scan-rate-independent conditions were established.

To calculate the TOF, FOWA was performed using CVs under acid saturated conditions. Herein, we report the average values of TOF recorded at three different scan rates after establishing the scan rate independence. FOWA was analyzed at scan rates of 7.0−9.0 V/s in ACN and 5.0−7.0 V/s in DMF solutions.

The CPC data were collected using a two-chambered glass electrolysis cell. The working compartment was fitted with a glassy carbon working electrode and Ag/Ag^+ reference electrode. The auxiliary compartment was fitted with a Pt wire counter electrode. The cell was washed and dried in an oven overnight before conducting the experiments. In a typical experiment, the working compartment was loaded with 0.30 mM catalyst, the desired acid (CH_3COOH or CF_3COOH) at saturation conditions, and 0.1 M TBAHFP in ACN or DMF solution. The auxiliary compartment was filled with a 0.1 M TBAHFP in ACN or DMF solution. Before electrolysis, both compartments were sparged with nitrogen for ∼15 min. Data was collected at a constant applied potential equal to the potential required for $i_{cat/2}$ in the CV studies. A control (blank) CPC study was conducted and subtracted from experimental results. A Gow-Mac series 400 GC-TCD fitted with a molecular sieve column heated to 130 °C was used for the detection of hydrogen gas in the head space of the CPC cell. Faradaic efficiency was determined using an inverted H-shaped cell in which the evolved gas displaced the volume of the solvent in the cathode compartment, calculated as $V = \pi(r)^2h$. The evolved moles of hydrogen can be quantified by the applying the conversion factor of 1 mol of gas corresponds to 22.4 L.

X-band electronic paramagnetic resonance (EPR) spectra was collected in frozen ACN at 77 K temperature using a Bruker EMX spectrometer. Electronic absorption spectra were recorded with an Agilent 8453 diode array spectrometer.

Computational Methods. The reliability of computed potential energy surface (PES) associated with particular reaction mechanism employing density functional theory (DFT) is largely dependent on the choice of the appropriate functional. To be consistent with the previous studies, calculations were performed using B3LYP a hybrid functional and BP86 a GGA-type functional, as these two functionals produce reliable agreement with experimental results.[22,39] Optimizations were performed in the gas as well as in solution employing PCM[65] and using the B3LYP and BP86 functionals[46−51] with 6-311g(d,p)[52] and TZV/P basis set.[53] The choice of the functional and basis set was made to directly compare the results obtained with the previously reported CuL^1 and NiL^2. In addition, natural bond orbital (NBO) analysis were performed and the reduction potentials of the redox events were computed using the B3LYP/6-311g(d,p) level of theory and compared with the experimental data.[54] Time-dependent DFT (TD-DFT) calculations were performed to simulate the absorption spectra of the neutral, monoreduced and direduced species.[39,55] All geometry optimizations were carried out under tight convergence criteria, with no symmetry imposed. All reported calculations were performed using Gaussian 09 software suite.[56] ChemCraft[57] and GaussView were used for the graphical presentation. All input coordinates are provided in the Supporting Information.

RESULTS AND DISCUSSION

Synthesis and Electrochemical Characterization. The NiL^1 complex is obtained in high yields as an air and moisture stable dark green solid by using previously reported methods.[40] The CV of NiL^1 in DMF solution displays two quasi-reversible events in the cathodic region from 0 to −2.80 vs Fc^+/Fc^0, as in Figure S1. The first event, $E_{1/2}$ = −1.83 V, is assigned to ligand centered reduction, $Ni(II)L^1/[Ni(II)L^1\cdot]^-$. A similar ligand-centered event is reported for NiL^2 at a potential of −1.64 V.[39] The second event for NiL^1 at −2.45 V is assigned as metal-centered $Ni^{II/I}$ couple, which is similar to the reported $Ni^{II/I}$ potential of −2.27 V for NiL^2. The irreversible oxidation event at −1.30 V for NiL^1 is only observed after scanning through the second reduction event. A similar unassigned feature is observed in the CV of NiL^2.[39] Analysis of the cathodic current for NiL^1 in DMF at the multiple scan rates from 0.1 to 0.5 V/s were used to construct a Cottrell plot, shown in Figure S1, establishing that the reduction is diffusion limited with a diffusion coefficient of 2.74×10^{-5} cm^2/s. The CV of NiL^1 in ACN displays a similar quasi-reversible ligand- and metal-centered events at −1.73 and −2.31 V, respectively, given in

DOI: 10.1021/acs.inorgchem.8b02110
Inorg. Chem. 2018, 57, 13486−13493

Figure 1. The diffusion coefficient for NiL[1] in ACN is 5.01 × 10^{-5} cm^2/s.

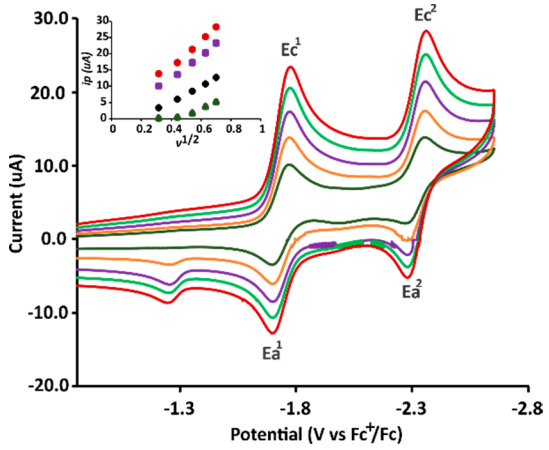

Figure 1. Scan rate dependent cyclic voltammograms of NiL[1] recorded at scan rates at 0.1 V/s (bottom) to 0.5 V/s (top) in ACN solutions with 0.1 M TBAHFP as supporting electrolyte. (Inset) Cottrell plot of peak current versus the square root of scan rate.[Ec^1 = purple squares, Ec^2 = red circles, Ea^1 = black circles, Ea^2 = green triangles].

Electrocatalytic Hydrogen Evolution: CV Studies. The performance of NiL[1] as an electrocatalyst for the hydrogen evolution reaction was evaluated under a series of four conditions in which the solvent (ACN or DMF) and proton source (CH_3COOH or CF_3COOH) were systematically varied. The acids and solvents in this study were chosen to directly compare the HER activity of NiL[1] with the previously reported complexes.[22,23,39,55,58] The highest TOF was observed in ACN with CH_3COOH. Notably, the lowest TOF for NiL[1] was observed in DMF with CF_3COOH, which were the only conditions reported for NiL[2].

The addition of CH_3COOH (p*Ka* = 23.51)[59] to NiL[1] in ACN introduced a catalytic current at −2.35 V vs Fc^+/Fc^0, given in Figure 2. Initially, the catalytic to peak current ratio (i_{cat}/i_p) increase linearly with increasing acid concentration. The value of i_{cat}/i_p saturates when the concentration of CH_3COOH reaches 12.60 mM. After establishing these acid

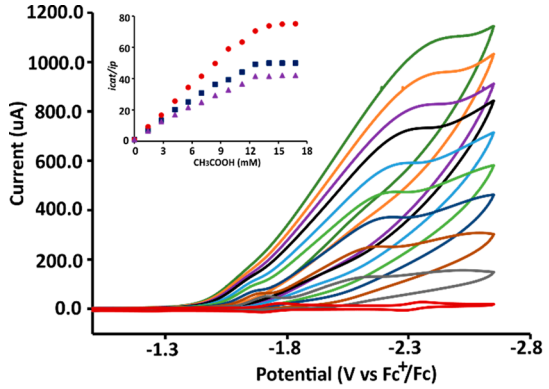

Figure 2. CVs of 0.30 mM NiL[1] in ACN solution with 0.1 M TBAHFP collected at scan rate of 0.5 V/s with 0, 1.4, 2.8, 4.2, 5.6, 7.0, 8.4, 9.8, 11.2, and 12.6 mM (top) CH_3COOH concentrations. Inset: Plot of i_{cat}/i_p vs [CH_3COOH] for 0.30 mM NiL[1] at scan rate of 0.2 (red circles), 0.5 (blue squares), and 1.0 (purple triangles) V/s.

saturated conditions, the scan rate was increased until the scan rate independent region was observed at 7.0 V/s. Using FOWA, a TOF of 4200 s^{-1} was determined with an overpotential of 0.53 V.

The electrocatalytic activity of NiL[1] in ACN was accessed using CF_3COOH (p*Ka* = 12.65)[60] as a proton source. As shown in Figure 3, there is an increase in the cathodic current

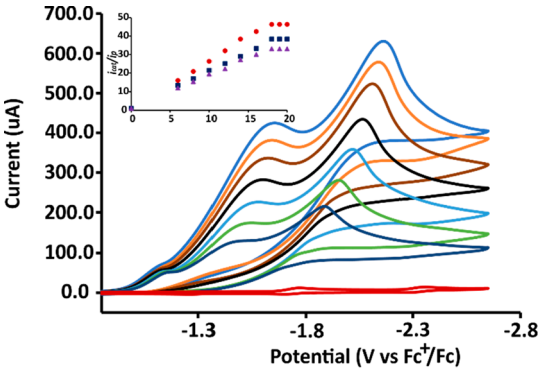

Figure 3. CVs of 0.30 mM NiL[1] in ACN solution with 0.1 M TBAHFP collected at scan rate of 0.2 V/s with 0, 6, 8, 10, 12, 14, 16, and 18 mM (top) CF_3COOH concentrations. Inset: Plot of i_{cat}/i_p vs [CF_3COOH] for 0.30 mM NiL[1] at scan rate of 0.2 (red circles), 0.5 (blue squares), and 1.0 (purple triangles) V/s.

at −1.65 V and −2.26 V vs Fc^+/Fc^0 upon successive additions of CF_3COOH. The presence of two catalytic waves suggests the mechanism is more complex than with CH_3COOH and may involve multiple pathways. For the sake of comparison, we will focus on the process occurring at the more cathodic potential ($E_{cat/2}$ = −1.90 V vs Fc^+/Fc^0). Acid saturation occurs when the concentration of CF_3COOH reaches 18.0 mM. Under acid saturating conditions, i_{cat} becomes scan rate independent at 7.0 V/s. Using FOWA, a TOF of 1300 s^{-1} is calculated with an overpotential of 0.67 V. The decrease in the HER activity with CF_3COOH may be attributed to differences in dimerization of the two acids in ACN. For example, the loss of dimerization of CF_3COOH due to heteroconjugation with water in ACN solutions has been shown to lower HER activity.[60]

Using a similar approach, the catalytic activity of NiL[1] for HER was evaluated in DMF with CH_3COOH and CF_3COOH. Successive additions of CH_3COOH (Figure 4) or CF_3COOH (Figure 5) to DMF solutions of NiL[1] showed increases in cathodic current at −2.62 and −2.10 V, respectively. Acid saturation occurs at 9.80 mM with CH_3COOH and 32.0 mM with CF_3COOH. Under scan-rate-independent conditions, 5.0 V/s, a TOF of 1200 s^{-1} at an overpotential of 0.85 V is observed with CH_3COOH, while a TOF of 120 s^{-1} is observed with CF_3COOH. The lower activity in DMF as compared to ACN solutions can be associated with the stabilizing hydrogen bonding interactions between the N−H groups in the ligand framework and the DMF solvent.[22]

Next, the order of the reaction with respect to the catalyst was evaluated. The catalytic current was measured at four different NiL[1] concentrations (0.125, 0.25, 0.50, and 0.75 mM) under acid saturating conditions of 12.6 mM CH_3COOH. A linear relationship was established upon plotting the i_{cat} versus [NiL^1], corresponding to a first-order dependence on the concentration of the catalyst, Figure S10.

DOI: 10.1021/acs.inorgchem.8b02110
Inorg. Chem. 2018, 57, 13486−13493

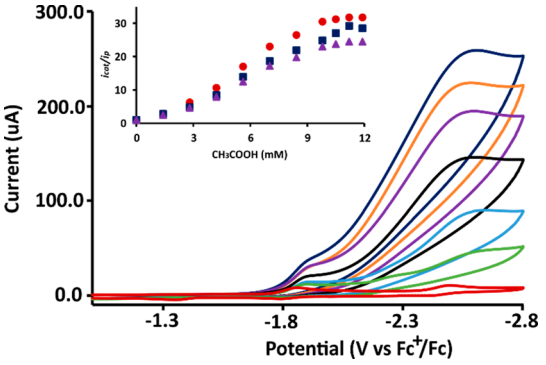

Figure 4. CVs of 0.30 mM NiL^1 in DMF solution 0.1 M TBAHFP collected at scan rate of 0.2 V/s with 0, 2.8, 4.2, 5.6, 7, 8.4, and 9.8 mM (top) CH_3COOH concentrations. Inset: Plot of i_{cat}/i_p vs [CH_3COOH] for 0.30 mM NiL^1 at scan rate of 0.2 (red circles), 0.5 (blue squares), and 1.0 (purple triangles) V/s.

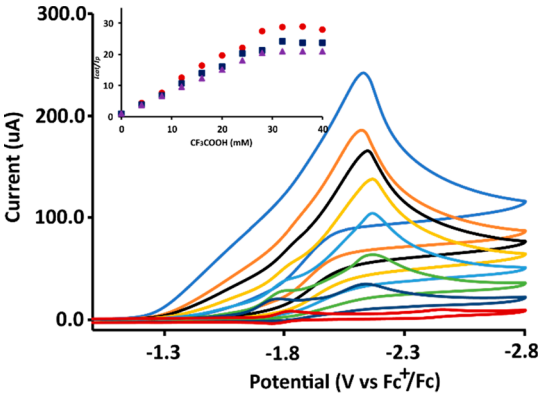

Figure 5. CVs of 0.30 mM NiL^1 in DMF solution with 0.1 M TBAHFP collected at scan rate of 0.2 V/s with 0, 4, 8, 12, 16, 20, 24, and 32 mM (top) CF_3COOH concentrations. Inset: Plot of i_{cat}/i_p vs [CF_3COOH] for 0.30 mM NiL^1 at scan rate of 0.2 (red circles), 0.5 (blue squares), and 1.0 (purple triangles) V/s.

To gain further insights into the mechanism, the kinetic isotopic effect for HER catalysis by NiL^1 was measured using deuterated acids.[22,24,61] In separate experiments, CV data were collected with 0.30 mM NiL^1 in ACN or DMF with successive additions of the deuterated acids CD_3CO_2D or CF_3CO_2D. For acetic acid, KIE (H/D) values of 0.75 and 0.64 were obtained in ACN and DMF, respectively. Slightly lower values of 0.54 and 0.57 were obtained for CF_3CO_2H/CF_3CO_2D in ACN and DMF, respectively. In all the cases, the value of KIE is less than one indicating an inverse isotope effect, which is similar to that reported from Gray and Fukuzumi for HER via a metal hydride intermediate.[62,63]

Electrocatalytic Hydrogen Evolution: CPC Studies. The stability of NiL^1 as an electrocatalyst for HER was evaluated in ACN and DMF by conducting CPC experiments over a period of 4 h, as in Figure 6 and Table 1. Electrolysis of ACN solutions containing 0.1 M TBAHFP, 0.30 mM NiL^1, and 12.60 mM CH_3COOH at a constant potential of −1.90 vs Fc^+/Fc^0 resulted in a total charge passed of 27.56 C, corresponding to 1.43×10^{-4} moles of H_2 produced with a turnover number (TON) of 48. Gas chromatography thermal conductivity (GC-TCD) was used to analyze the headspace sample confirming H_2 as the gaseous product. Similar experiments with CF_3COOH (18.0 mM) for 4 h yielded a net charge of 13.67 C associated with a TON of 24. The lower

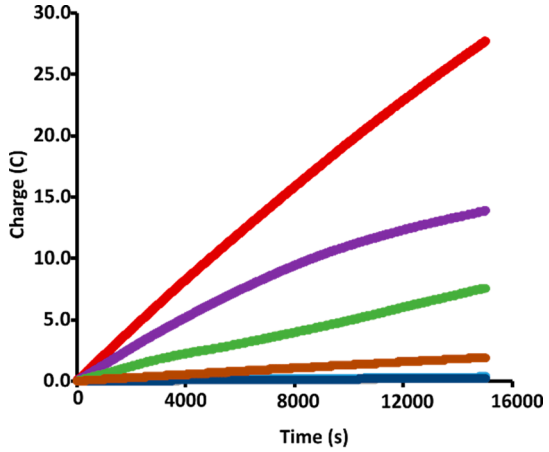

Figure 6. CPC of 0.30 mM NiL^1 in 0.1 M TBAHFP with 12.6 mM CH_3COOH (red), 18.0 mM CF_3COOH (purple) in ACN solutions, with 9.8 mM CH_3COOH (green), 32.0 mM CF_3COOH (brown) in DMF solutions. CPC with no NiL^1 in 0.1 M TBAHFP with 9.8 mM CH_3COOH (light blue), and 32.0 mM CF_3COOH (blue) in DMF solutions.

Table 1. CPC Results

entry	solvent	acid	q (C)	n ($\times 10^{-4}$)	TON
1	ACN	CH_3COOH	27.56	1.43	48
2	ACN	CF_3COOH	13.67	0.71	24
3	DMF	CH_3COOH	7.26	0.38	13
4	DMF	CF_3COOH	1.69	0.087	3

TON relative to CH_3COOH is consistent with the lower TOF. The same trend is observed for CPC data collected in DMF solution. With CH_3COOH (9.80 mM) a TON of 13 is obtained after 4 h in DMF. When the proton source in DMF is changed to CF_3COOH (32 mM), the TON is lowered to 3. The relatively low TON, with respect to the TOF, is attributed to the fact that only catalyst at the electrode surface is actively generating the hydrogen, but the bulk concentration of the catalyst is used to calculate the TON values.

Electrocatalytic Hydrogen Evolution: Control Experiments. To confirm that the HER observed is associated with NiL^1 in solution and not due to surface adsorbed complex or degradation products, a series of control experiments have been undertaken. First, blank CVs collected in the presence of CH_3COOH or CF_3COOH without the addition of NiL^1 showed no measurable current at potentials associated with hydrogen evolution (Figures S15−S18). A series of CVs were recorded with NiL^1 in ACN or DMF in the presence of acid to confirm HER activity. Then, the glassy carbon working electrode was removed from solution and washed with the deionized water but not polished. Immersion of the electrode into a fresh working solution containing acid and electrolyte showed no observable catalytic current upon sweeping the potential in the cathodic region. This indicates that HER activity is due neither to a film of the catalyst nor its degradation product being strongly absorbed on the electrode surface. To further probe whether the film formation on the working electrode surface was responsible for catalysis, a dip test was performed after CPC (Figure S19).[23,61,64]

To probe if the first step of catalysis could involve protonation of the catalyst, the titration of NiL^1 with acid was monitored in the UV−visible region.[22] The electronic spectra of NiL^1 in ACN or DMF did not significantly change

DOI: 10.1021/acs.inorgchem.8b02110
Inorg. Chem. 2018, 57, 13486−13493

upon the addition of either CH_3COOH or CF_3COOH. The results are consistent with a mechanism in which reduction of NiL^1 is required prior to protonation. Reduction of NiL^1 in ACN with cobaltocene to $[NiL^1]^-$ yields an $S = 1/2$ radical species. The EPR spectrum of $[NiL^1]^-$ displays a rhombic signal with a narrow g-value spread, $g_1 = 2.02$, $g_2 = 2.00$, and $g_3 = 1.983$, that is inconsistent with a Ni(I) assignment (Figure S26). The average g-value of 2.003 indicates the reduction is ligand-centered.[37] Addition of CF_3COOH to the reduced sample results in no significant change in g-values indicating that the radical of $Ni(HL^1\cdot)$ remains ligand centered confirming ligand-centered protonation.

Proposed Homogeneous HER Mechanism. A proposed ECEC (E = electron transfer, C = chemical reaction; i.e., protonation) mechanism for HER is shown in Scheme 2. The

Scheme 2. Proposed HER Mechanism with NiL^1

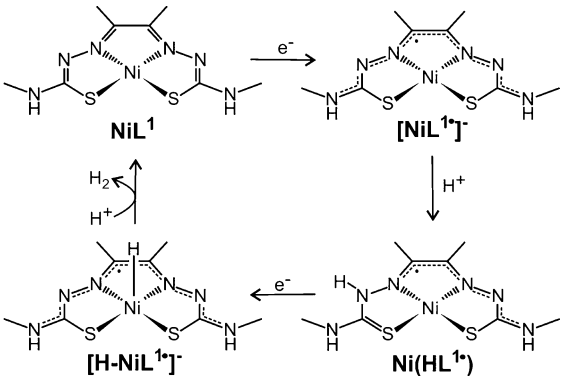

mechanism is supported by computational investigations as described below. An alternate, EECC mechanism cannot be completely excluded. In either case, the first step of the cycle is ligand centered reduction of NiL^1 by one electron to yield $[Ni(II)L^1\cdot]^-$. Protonation of $[Ni(II)L^1\cdot]^-$ occurs at a non-coordinated hydrazino-N to generate $Ni(II)(HL^1\cdot)$. Reduction of $Ni(II)(HL^1\cdot)$ yields the metal hydride species, $[HNi(III)\text{-}L^1\cdot]^-$, which reacts with external proton in the solution to generate hydrogen. The mechanism is consistent with experimental results that indicate the reaction is first-order with respect to the catalyst. Additionally, the catalysis requires reduction prior to protonation, and the KIE is consistent with the formation of a metal hydride. The proposed mechanism involves four key Ni complexes that were evaluated by DFT investigations.

Computational Studies. The proposed complexes in Scheme 2 were optimized by DFT using the B3LYP functional[49,50] with the 6-311g(d,p)[52] basis set and the BP86 functional[46−48] with the TZV/P basis set.[53] The former was previously used by our group to investigate the HER catalysis by CuL^1,[22] while the latter was employed by Straistari et al. for NiL^2.[39] Geometry optimization were carried out in gas phase, as well as in solution phase using PCM.[65]

The neutral NiL^1 catalyst model was optimized as a restricted singlet ($S = 0$) using initial geometrical parameters taken from the previously reported crystal structure.[66] The optimized metal−ligand bond distances and angles are within 0.1 Å and 2.2°, respectively, of the experimental values (see Table S1). Reduction of NiL^1 by one electron yields a doublet electronic state ($S = 1/2$) best described as the Ni(II)-ligand radical $[NiL^1\cdot]^-$ with 95% of the spin density on the ligand framework as determined with B3LYP/6-311g(d,p) in the solution phase. Similar results were obtained in the gas phase using B3LYP/6-311g(d,p) and with BP86/TZV/P in the gas and solution phases. The assignment of the first reduction as ligand centered is consistent with the previously reported calculations of $[NiL^2\cdot]^-$.[39] On the basis of the spin density distribution, the second reduction is assigned to be metal-centered reduction from Ni(II) to Ni(I) (Figure S28).

The theoretical prediction of the standard redox potentials for both reduction events in ACN solutions was obtained using Born−Haber cycle with B3LYP/6-311g(d,p) (Scheme S1). The standard ferrocene couple ($Fc^+/Fc^0 = 4.988$) was used as a reference electrode.[67] The first reduction which is assigned as ligand-centered reduction was computed to be −2.04 V, while the second reduction event assigned as metal-centered was predicted to be −2.55 V (Table S3). These values were found to be in good agreement with the experimental values ($E_c^1 = -1.73$ V and $E_c^2 = -2.31$ V) considering that the computation of reduction potential using B3LYP functionals requires a consistent shift of −0.48 V.[68]

TD-DFT calculations were performed to simulate the neutral and the reduced species of NiL^1 (Figure S29). The absorption spectrum is dominated by one major band in the range of 300−500 nm consistent with experimental data. In neutral NiL^1 absorption band at 386 nm was assigned to the electronic transition from mixed metal−ligand to ligand orbitals. For monoreduced and direduced species band at 390 and 446 nm demonstrates ligand to ligand and metal−ligand to ligand orbital transition, respectively (Table S2).

Protonation of $[NiL^1\cdot]^-$ can potentially occur at Ni, S, N^2 (hydrazino), N^1(coordinated), or N^3 (pendant amine). Each of these sites were evaluated in the doublet ground state ($S = 1/2$). The calculations based on B3LYP/6-311g(d,p) solution phase, given in Figure 7, favor protonation at the N^2 (hydrazino) relative to N^1 (coordinated) by 2.85 kcal/mol. All other protonation sites are disfavored by at least 12.56 kcal/mol. The solution phase computed using BP86/TZV/P also favors protonation at N^2 over N^1 (5.95 kcal/mol; Figure S43). Notably, gas phase calculations show nearly degenerate

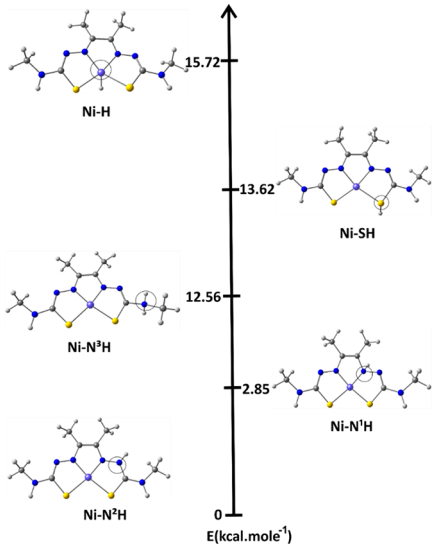

Figure 7. Energetic stability of the reduced/protonated species, $Ni(HL^1\cdot)$, ($S = 1/2$, $q = 0$), B3LYP/6-311g(d, p) solution phase calculations in ACN.

DOI: 10.1021/acs.inorgchem.8b02110
Inorg. Chem. 2018, 57, 13486−13493

energies for protonation at N^1 and N^2, (Figures S30 and S40). Our results somehow are different than those those of Straistari, which report preferential protonation at N^1 by 4 kcal/mol over N^2.[39]

The reduction of Ni(HL^1·) is complicated as it could result in a singlet (S = 0) or triplet (S = 1) species and may involve shifting of the proton from N^2.[22] The resulting complex was evaluated in the solution phase using B3LYP/6-311g(d,p) at multiple protonation sites in both spin states (Figure S33). The structures corresponding to singlet states are discounted based on the relatively high energies required for the H_2 evolving step (see the Supporting Information). Representations of the lowest energy triplet structures are provided in Figure 8. The lowest energy structure is the 5-coordinate,

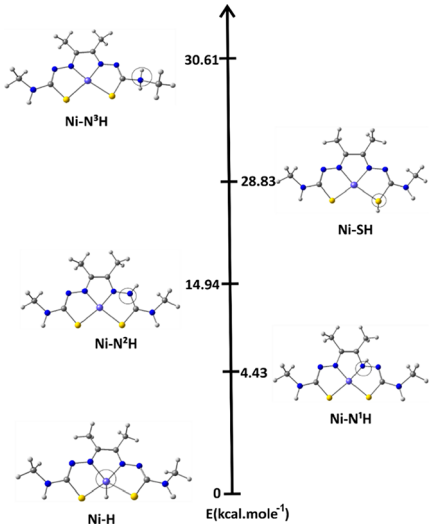

Figure 8. Energetic stability of the reduced/protonated/reduced species, $[Ni(HL^1\cdot)]^-$, (S = 1, q = −1) B3LYP/6-311g(d, p) solution phase calculations in ACN.

metal hydride $[HNi(L^1\cdot)]^-$. It is best described as Ni(III)-H coordinated to the ligand radical $(L^1\cdot)^{3-}$. The next lowest energy complex, which is protonated at N^1, sits 4.43 kcal/mol higher in energy. It is analogous to the lowest energy structure reported by Straistari for $[Ni(HL^2)]^-$.[39] All other protonation sites are significantly higher in energy.

The natural bond orbital (NBO) analysis was performed on the lowest energy $[HNi(L^1\cdot)]^-$ structure.[54] The result indicates the formation of the NiH^- (Figure S39). Considering the NBO results, the final step of catalysis involves the reaction of $[HNi(L^1\cdot)]^-$ with H^+ generating H_2. The reaction occurs without the second protonation of the ligand. The transition state (TS) involving the H_2 evolution was located using the B3LYP/6-311g(d,p) in solution modeled via PCM (Figure 9) and characterized by a single imaginary frequency of i 1786 cm^{-1}. The relatively low energy barrier of 10.5 kcal/mol of TS supports the formation of hydrogen from the $[H\text{-}NiL^1\cdot]^-$ on interaction with the external proton from the acid in the solution.

CONCLUSION

The redox active framework of thiosemicarbazone ligands can serve as a charge carrier for electrocatalysis in the presence or absence of a transition metal ion. With respect to HER, both the ligand and the metal of thiosemicarbazone complexes can

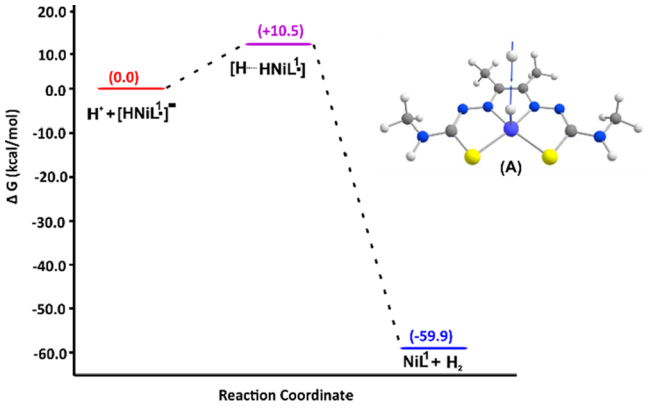

Figure 9. Energy profile and transition state for hydrogen evolution with NiL^1. (A) TS representation $[H\cdots HNiL^1\cdot]$.

serve as the site of proton reduction. As we have detailed previously, the HER mechanism for metal bis-(thiosemicarbazone) complexes depends on the number of d-electrons and the relative energy of the ligand- and metal-centered orbitals. Previously, our group reported strictly ligand-centered HER for ZnL^1 with the metal serving a structural role.[23] All reductions and bond making/breaking reactions occur on the ligand. In contrast, HER with CuL^1 occurs through metal-assisted ligand-centered reactivity.[22] The bond making/breaking reactions remain on the ligand center, but the metal serves as an electron reservoir. Recently, Straistari et al. reported PdL^2 as a HER catalyst that is proposed to follow the same mechanism as CuL^1.[58] In the current paper, we report that bond breaking/making shifts from the ligand to the metal center for NiL^1. In this ligand-assisted metal-centered reaction, the ligand serves as the electron reservoir. The mechanism is consistent with the suggestion that a catalytically active Ni(III)-H is responsible for H_2 evolution with NiL^2. Further, the results of the current manuscript provide the first DFT support of a Ni(III)-H as an intermediate on the reaction surface for HER. A metal hydride pathway was also anticipated for CoL^2, although that remains to be confirmed.[55]

ASSOCIATED CONTENT

Supporting Information

The Supporting Information is available free of charge on the ACS Publications website at DOI: 10.1021/acs.inorgchem.8b02110.

Sample calculations, supplementary CV data, plots of FOWA analysis, EPR spectra, DFT details of B3LYP/6-311g(d,p) gas phase, BP86/TZV/P (gas and solution) and computational input coordinates (PDF)

AUTHOR INFORMATION

Corresponding Author

*E-mail: craig.grapperhaus@louisville.edu.

ORCID

Abdullah Al Mamun: 0000-0001-8941-8195

Pawel M. Kozlowski: 0000-0002-4090-8078

Craig A. Grapperhaus: 0000-0003-4889-2645

Notes

The authors declare no competing financial interest.

DOI: 10.1021/acs.inorgchem.8b02110
Inorg. Chem. 2018, 57, 13486−13493

■ ACKNOWLEDGMENTS

This research was supported in part by the National Science Foundation (CHE-1665136) and a grant from the Kentucky Science and Engineering Foundation as per grant agreement no. KSEF-148-502-15-350 with the Kentucky Science and Technology Corporation. We are thankful to Cardinal Research Cluster at the University of Louisville for providing the computational facilities. We thank Mr. Nicholas Vishnosky for assistance with electrochemical experiments.

■ REFERENCES

(1) Cook, T. R.; Dogutan, D. K.; Reece, S. Y.; Surendranath, Y.; Teets, T. S.; Nocera, D. G. Solar Energy Supply and Storage for the Legacy and Nonlegacy Worlds. *Chem. Rev.* **2010**, *110*, 6474−6502.
(2) DuBois, D. L. Development of Molecular Electrocatalysts for Energy Storage. *Inorg. Chem.* **2014**, *53*, 3935−3960.
(3) Nocera, D. G. The Artificial Leaf. *Acc. Chem. Res.* **2012**, *45*, 767−776.
(4) Teets, T. S.; Nocera, D. G. Photocatalytic hydrogen production. *Chem. Commun.* **2011**, *47*, 9268−9274.
(5) Vesborg, P. C. K.; Seger, B.; Chorkendorff, I. Recent Development in Hydrogen Evolution Reaction Catalysts and Their Practical Implementation. *J. Phys. Chem. Lett.* **2015**, *6*, 951−957.
(6) Mehta, V.; Cooper, J. S. Review and analysis of PEM fuel cell design and manufacturing. *J. Power Sources* **2003**, *114*, 32−53.
(7) Goldet, G.; Wait, A. F.; Cracknell, J. A.; Vincent, K. A.; Ludwig, M.; Lenz, O.; Friedrich, B.; Armstrong, F. A. Hydrogen Production under Aerobic Conditions by Membrane-Bound Hydrogenases from Ralstonia Species. *J. Am. Chem. Soc.* **2008**, *130*, 11106−11113.
(8) Jones, A. K.; Sillery, E.; Albracht, S. P. J.; Armstrong, F. A. Direct comparison of the electrocatalytic oxidation of hydrogen by an enzyme and a platinum catalyst. *Chem. Commun.* **2002**, 866−867.
(9) Vincent, K. A.; Belsey, N. A.; Lubitz, W.; Armstrong, F. A. Rapid and Reversible Reactions of [NiFe]-Hydrogenases with Sulfide. *J. Am. Chem. Soc.* **2006**, *128*, 7448−7449.
(10) Vincent, K. A.; Cracknell, J. A.; Lenz, O.; Zebger, I.; Friedrich, B.; Armstrong, F. A. Electrocatalytic hydrogen oxidation by an enzyme at high carbon monoxide or oxygen levels. *Proc. Natl. Acad. Sci. U. S. A.* **2005**, *102*, 16951−16954.
(11) Holton, O. T.; Stevenson, J. W. The role of Platinum in Proton Exchange Membrane Fuel Cells. *Platinum Met. Rev.* **2013**, *57*, 259−271.
(12) Rakowski DuBois, M.; DuBois, D. L. The roles of the first and second coordination spheres in the design of molecular catalysts for H2 production and oxidation. *Chem. Soc. Rev.* **2009**, *38*, 62−72.
(13) McKone, J. R.; Marinescu, S. C.; Brunschwig, B. S.; Winkler, J. R.; Gray, H. B. Earth-abundant hydrogen evolution electrocatalysts. *Chem. Sci.* **2014**, *5*, 865−878.
(14) Gan, L.; Groy, T. L.; Tarakeshwar, P.; Mazinani, S. K. S.; Shearer, J.; Mujica, V.; Jones, A. K. A Nickel Phosphine Complex as a Fast and Efficient Hydrogen Production Catalyst. *J. Am. Chem. Soc.* **2015**, *137*, 1109−1115.
(15) Rakowski DuBois, M.; DuBois, D. L. Development of Molecular Electrocatalysts for CO2 Reduction and H2 Production/Oxidation. *Acc. Chem. Res.* **2009**, *42*, 1974−1982.
(16) McNamara, W. R.; Han, Z.; Alperin, P. J.; Brennessel, W. W.; Holland, P. L.; Eisenberg, R. A Cobalt−Dithiolene Complex for the Photocatalytic and Electrocatalytic Reduction of Protons. *J. Am. Chem. Soc.* **2011**, *133*, 15368−15371.
(17) Berben, L. A.; Peters, J. C. Hydrogen evolution by cobalt tetraimine catalysts adsorbed on electrode surfaces. *Chem. Commun.* **2010**, *46*, 398−400.
(18) Mejia-Rodriguez, R.; Chong, D.; Reibenspies, J. H.; Soriaga, M. P.; Darensbourg, M. Y. The Hydrophilic Phosphatriazaadamantane Ligand in the Development of H2 Production Electrocatalysts: Iron Hydrogenase Model Complexes. *J. Am. Chem. Soc.* **2004**, *126*, 12004−12014.
(19) Jurss, J. W.; Khnayzer, R. S.; Panetier, J. A.; El Roz, K. A.; Nichols, E. M.; Head-Gordon, M.; Long, J. R.; Castellano, F. N.; Chang, C. J. Bioinspired design of redox-active ligands for multielectron catalysis: effects of positioning pyrazine reservoirs on cobalt for electro- and photocatalytic generation of hydrogen from water. *Chem. Sci.* **2015**, *6*, 4954−4972.
(20) Thompson, E. J.; Berben, L. A. Electrocatalytic Hydrogen Production by an Aluminum(III) Complex: Ligand-Based Proton and Electron Transfer. *Angew. Chem., Int. Ed.* **2015**, *54*, 11642−11646.
(21) Sherbow, T. J.; Fettinger, J. C.; Berben, L. A. Control of Ligand pKa Values Tunes the Electrocatalytic Dihydrogen Evolution Mechanism in a Redox-Active Aluminum(III) Complex. *Inorg. Chem.* **2017**, *56*, 8651−8660.
(22) Haddad, A. Z.; Cronin, S. P.; Mashuta, M. S.; Buchanan, R. M.; Grapperhaus, C. A. Metal-Assisted Ligand-Centered Electrocatalytic Hydrogen Evolution upon Reduction of a Bis(thiosemicarbazonato)-Cu(II) Complex. *Inorg. Chem.* **2017**, *56*, 11254−11265.
(23) Haddad, A. Z.; Garabato, B. D.; Kozlowski, P. M.; Buchanan, R. M.; Grapperhaus, C. A. Beyond Metal-Hydrides: Non-Transition-Metal and Metal-Free Ligand-Centered Electrocatalytic Hydrogen Evolution and Hydrogen Oxidation. *J. Am. Chem. Soc.* **2016**, *138*, 7844−7847.
(24) Haddad, A. Z.; Kumar, D.; Ouch Sampson, K.; Matzner, A. M.; Mashuta, M. S.; Grapperhaus, C. A. Proposed Ligand-Centered Electrocatalytic Hydrogen Evolution and Hydrogen Oxidation at a Noninnocent Mononuclear Metal−Thiolate. *J. Am. Chem. Soc.* **2015**, *137*, 9238−9241.
(25) Zhang, W.; Haddad, A. Z.; Garabato, B. D.; Kozlowski, P. M.; Buchanan, R. M.; Grapperhaus, C. A. Translation of Ligand-Centered Hydrogen Evolution Reaction Activity and Mechanism of a Rhenium-Thiolate from Solution to Modified Electrodes: A Combined Experimental and Density Functional Theory Study. *Inorg. Chem.* **2017**, *56*, 2177−2187.
(26) Panetier, J. A.; Letko, C. S.; Tilley, T. D.; Head-Gordon, M. Computational Characterization of Redox Non-Innocence in Cobalt-Bis(Diaryldithiolene)-Catalyzed Proton Reduction. *J. Chem. Theory Comput.* **2016**, *12*, 223−230.
(27) Lyaskovskyy, V.; de Bruin, B. Redox Non-Innocent Ligands: Versatile New Tools to Control Catalytic Reactions. *ACS Catal.* **2012**, *2*, 270−279.
(28) Jing, X.; Wu, P.; Liu, X.; Yang, L.; He, C.; Duan, C. Light-driven hydrogen evolution with a nickel thiosemicarbazone redox catalyst featuring Ni···H interactions under basic conditions. *New J. Chem.* **2015**, *39*, 1051−1059.
(29) Wise, C. F.; Liu, D.; Mayer, K. J.; Crossland, P. M.; Hartley, C. L.; McNamara, W. R. A nickel complex of a conjugated bis-dithiocarbazate Schiff base for the photocatalytic production of hydrogen. *Dalton Trans* **2015**, *44*, 14265−14271.
(30) Blanchard, S.; Bill, E.; Weyhermüller, T.; Wieghardt, K. N. N-Coordinated π Radical Anions of S-Methyl-1-phenyl-isothiosemicarbazide in Two Five-Coordinate Ferric Complexes [FeIII(LMe•)2X] (X = CH3S-, Cl-). *Inorg. Chem.* **2004**, *43*, 2324−2329.
(31) Blanchard, S.; Neese, F.; Bothe, E.; Bill, E.; Weyhermüller, T.; Wieghardt, K. Square Planar vs Tetrahedral Coordination in Diamagnetic Complexes of Nickel(II) Containing Two Bidentate π-Radical Monoanions. *Inorg. Chem.* **2005**, *44*, 3636−3656.
(32) Akbar Ali, M.; Bernhardt, P. V.; Brax, M. A. H.; England, J.; Farlow, A. J.; Hanson, G. R.; Yeng, L. L.; Mirza, A. H.; Wieghardt, K. The Trivalent Copper Complex of a Conjugated Bis-dithiocarbazate Schiff Base: Stabilization of Cu in Three Different Oxidation States. *Inorg. Chem.* **2013**, *52*, 1650−1657.
(33) Kowol, C. R.; Reisner, E.; Chiorescu, I.; Arion, V. B.; Galanski, M.; Deubel, D. V.; Keppler, B. K. An Electrochemical Study of Antineoplastic Gallium, Iron and Ruthenium Complexes with Redox Noninnocent α-N-Heterocyclic Chalcogensemicarbazones. *Inorg. Chem.* **2008**, *47*, 11032−11047.
(34) Cowley, A. R.; Dilworth, J. R.; Donnelly, P. S.; Labisbal, E.; Sousa, A. An Unusual Dimeric Structure of a Cu(I) Bis-(thiosemicarbazone) Complex: Implications for the Mechanism of

DOI: 10.1021/acs.inorgchem.8b02110
Inorg. Chem. 2018, 57, 13486−13493

Hypoxic Selectivity of the Cu(II) Derivatives. *J. Am. Chem. Soc.* **2002**, *124*, 5270−5271.
(35) Cowley, A. R.; Dilworth, J. R.; Donnelly, P. S.; White, J. M. Copper Complexes of Thiosemicarbazone−Pyridylhydrazine (THYNIC) Hybrid Ligands: A New Versatile Potential Bifunctional Chelator for Copper Radiopharmaceuticals. *Inorg. Chem.* **2006**, *45*, 496−498.
(36) Ashfield, L. J.; Cowley, A. R.; Dilworth, J. R.; Donnelly, P. S. Functionalized Thiosemicarbazone Clusters of Copper(I) and Silver(I). *Inorg. Chem.* **2004**, *43*, 4121−4123.
(37) Kochem, A.; Gellon, G.; Jarjayes, O.; Philouze, C.; du Moulinet d'Hardemare, A.; van Gastel, M.; Thomas, F. Nickel(ii) radical complexes of thiosemicarbazone ligands appended by salicylidene, aminophenol and aminothiophenol moieties. *Dalton Trans* **2015**, *44*, 12743−12756.
(38) Yusof, E. N. M.; Ravoof, T. B. S. A.; Tahir, M. I. M.; Jotani, M. M.; Tiekink, E. R. T. Bis{4-methylbenzyl 2-[4-(propan-2-yl)-benzylidene]hydrazinecarbodithioato-[kappa]2N2,S}nickel(II): crystal structure and Hirshfeld surface analysis. *Acta Crystallogr. E* **2017**, *73*, 397−402.
(39) Straistari, T.; Fize, J.; Shova, S.; Réglier, M.; Artero, V.; Orio, M. A Thiosemicarbazone−Nickel(II) Complex as Efficient Electrocatalyst for Hydrogen Evolution. *ChemCatChem* **2017**, *9*, 2262−2268.
(40) West, D. X.; Ives, J. S.; Bain, G. A.; Liberta, A. E.; Valdés-Martínez, J.; Ebert, K. H.; Hernández-Ortega, S. Copper(II) and nickel(II) complexes of 2,3-butanedione bis(N(3)-substituted thiosemicarbazones). *Polyhedron* **1997**, *16*, 1895−1905.
(41) Fourmond, V.; Jacques, P.-A.; Fontecave, M.; Artero, V. H2 Evolution and Molecular Electrocatalysts: Determination of Overpotentials and Effect of Homoconjugation. *Inorg. Chem.* **2010**, *49*, 10338−10347.
(42) Costentin, C.; Drouet, S.; Robert, M.; Savéant, J.-M. Turnover Numbers, Turnover Frequencies, and Overpotential in Molecular Catalysis of Electrochemical Reactions. Cyclic Voltammetry and Preparative-Scale Electrolysis. *J. Am. Chem. Soc.* **2012**, *134*, 11235−11242.
(43) Costentin, C.; Robert, M.; Saveant, J.-M. Catalysis of the electrochemical reduction of carbon dioxide. *Chem. Soc. Rev.* **2013**, *42*, 2423−2436.
(44) Costentin, C.; Savéant, J.-M. Multielectron, Multistep Molecular Catalysis of Electrochemical Reactions: Benchmarking of Homogeneous Catalysts. *ChemElectroChem* **2014**, *1*, 1226−1236.
(45) DiRisio, R. J.; Armstrong, J. E.; Frank, M. A.; Lake, W. R.; McNamara, W. R. Cobalt Schiff-base complexes for electrocatalytic hydrogen generation. *Dalton Trans* **2017**, *46*, 10418−10425.
(46) Perdew, J. P. Density-functional approximation for the correlation energy of the inhomogeneous electron gas. *Phys. Rev. B: Condens. Matter Mater. Phys.* **1986**, *33*, 8822−8824.
(47) Perdew, J. P. Erratum: Density-functional approximation for the correlation energy of the inhomogeneous electron gas. *Phys. Rev. B: Condens. Matter Mater. Phys.* **1986**, *34*, 7406−7406.
(48) Becke, A. D. Density-functional exchange-energy approximation with correct asymptotic behavior. *Phys. Rev. A: At., Mol., Opt. Phys.* **1988**, *38*, 3098−3100.
(49) Becke, A. D. A new mixing of Hartree−Fock and local density-functional theories. *J. Chem. Phys.* **1993**, *98*, 1372−1377.
(50) Lee, C.; Yang, W.; Parr, R. G. Development of the Colle-Salvetti correlation-energy formula into a functional of the electron density. *Phys. Rev. B: Condens. Matter Mater. Phys.* **1988**, *37*, 785−789.
(51) Gill, P. M. W.; Johnson, B. G.; Pople, J. A.; Frisch, M. J. The performance of the Becke—Lee—Yang—Parr (B—LYP) density functional theory with various basis sets. *Chem. Phys. Lett.* **1992**, *197*, 499−505.
(52) Wong, M. W.; Gill, P. M. W.; Nobes, R. H.; Radom, L. 6-311G(MC)(d, p): a second-row analogue of the 6-311G(d, p) basis set: calculated heats of formation for second-row hydrides. *J. Phys. Chem.* **1988**, *92*, 4875−4880.
(53) Schäfer, A.; Huber, C.; Ahlrichs, R. Fully optimized contracted Gaussian basis sets of triple zeta valence quality for atoms Li to Kr. *J. Chem. Phys.* **1994**, *100*, 5829−5835.
(54) Foster, J. P.; Weinhold, F. Natural hybrid orbitals. *J. Am. Chem. Soc.* **1980**, *102*, 7211−7218.
(55) Straistari, T.; Hardre, R.; Fize, J.; Shova, S.; Giorgi, M.; Reglier, M.; Artero, V.; Orio, M. Hydrogen Evolution Reactions Catalyzed by a Bis(thiosemicarbazone) Cobalt Complex: An Experimental and Theoretical Study. *Chem. - Eur. J.* **2018**, *24*, 8779−8786.
(56) Frisch, M. J.; Trucks, G. W.; Schlegel, H. B.; Scuseria, G. E.; Robb, M. A.; Cheeseman, J. R.; Scalmani, G.; Barone, V.; Petersson, G. A.; Nakatsuji, H.; Li, X.; Caricato, M.; Marenich, A. V.; Bloino, J.; Janesko, B. G.; Gomperts, R.; Mennucci, B.; Hratchian, H. P.; Ortiz, J. V.; Izmaylov, A. F.; Sonnenberg, J. L.; Williams-Young, D.; Ding, F.; Lipparini, F.; Egidi, F.; Goings, J.; Peng, B.; Petrone, A.; Henderson, T.; Ranasinghe, D.; Zakrzewski, V. G.; Gao, J.; Rega, N.; Zheng, G.; Liang, W.; Hada, M.; Ehara, M.; Toyota, K.; Fukuda, R.; Hasegawa, J.; Ishida, M.; Nakajima, T.; Honda, Y.; Kitao, O.; Nakai, H.; Vreven, T.; Throssell, K.; Montgomery, J. A., Jr.; Peralta, J. E.; Ogliaro, F.; Bearpark, M.; Heyd, J. J.; Brothers, E. N.; Kudin, K. N.; Staroverov, V. N.; Kobayashi, R.; Normand, J.; Raghavachari, K.; Rendell, A.; Burant, J. C.; Iyengar, S. S.; Tomasi, J.; Cossi, M.; Millam, J. M.; Klene, M.; Adamo, C.; Cammi, R.; Ochterski, J. W.; Martin, R. L.; Morokuma, K.; Farkas, O.; Foresman, J. B.; Fox, D. J. *Gaussian 16*, revision B.01; Gaussian, Inc.: Wallingford CT, 2016.
(57) Andrienko, G. *ChemCraft Visualization Software* http://www.chemcraftprog.com.
(58) Straistari, T.; Hardre, R.; Massin, J.; Attolini, M.; Faure, B.; Giorgi, M.; Reglier, M.; Orio, M. Influence of the Metal Ion on the Electrocatalytic Hydrogen Production by a Thiosemicarbazone Palladium Complex. *Eur. J. Inorg. Chem.* **2018**, *2018*, 2259−2266.
(59) Raamat, E.; Kaupmees, K.; Ovsjannikov, G.; Trummal, A.; Kütt, A.; Saame, J.; Koppel, I.; Kaljurand, I.; Lipping, L.; Rodima, T.; Pihl, V.; Koppel, I. A.; Leito, I. Acidities of strong neutral Brønsted acids in different media. *J. Phys. Org. Chem.* **2013**, *26*, 162−170.
(60) Rountree, E. S.; Dempsey, J. L. Reactivity of Proton Sources with a Nickel Hydride Complex in Acetonitrile: Implications for the Study of Fuel-Forming Catalysts. *Inorg. Chem.* **2016**, *55*, 5079−5087.
(61) Jain, R.; Mashuta, M. S.; Buchanan, R. M.; Grapperhaus, C. A. Electrocatalytic Hydrogen Evolution and Hydrogen Oxidation with a Ni(PS)2 Complex. *Eur. J. Inorg. Chem.* **2017**, *2017*, 3714−3719.
(62) Kotani, H.; Hanazaki, R.; Ohkubo, K.; Yamada, Y.; Fukuzumi, S. Size- and Shape-Dependent Activity of Metal Nanoparticles as Hydrogen-Evolution Catalysts: Mechanistic Insights into Photocatalytic Hydrogen Evolution. *Chem. - Eur. J.* **2011**, *17*, 2777−2785.
(63) Marinescu, S. C.; Winkler, J. R.; Gray, H. B. Molecular mechanisms of cobalt-catalyzed hydrogen evolution. *Proc. Natl. Acad. Sci. U. S. A.* **2012**, *109*, 15127−15131.
(64) Martin, D. J.; McCarthy, B. D.; Donley, C. L.; Dempsey, J. L. Electrochemical hydrogenation of a homogeneous nickel complex to form a surface adsorbed hydrogen-evolving species. *Chem. Commun.* **2015**, *51*, 5290−5293.
(65) Scalmani, G.; Frisch, M. J. Continuous surface charge polarizable continuum models of solvation. I. General formalism. *J. Chem. Phys.* **2010**, *132*, 114110.
(66) Blower, P. J.; Castle, T. C.; Cowley, A. R.; Dilworth, J. R.; Donnelly, P. S.; Labisbal, E.; Sowrey, F. E.; Teat, S. J.; Went, M. J. Structural trends in copper(ii) bis(thiosemicarbazone) radiopharmaceuticals. *Dalton Trans* **2003**, 4416−4425.
(67) Namazian, M.; Lin, C. Y.; Coote, M. L. Benchmark Calculations of Absolute Reduction Potential of Ferricinium/Ferrocene Couple in Nonaqueous Solutions. *J. Chem. Theory Comput.* **2010**, *6*, 2721−2725.
(68) Roy, L. E.; Jakubikova, E.; Guthrie, M. G.; Batista, E. R. Calculation of One-Electron Redox Potentials Revisited. Is It Possible to Calculate Accurate Potentials with Density Functional Methods? *J. Phys. Chem. A* **2009**, *113*, 6745−6750.

DOI: 10.1021/acs.inorgchem.8b02110
Inorg. Chem. 2018, 57, 13486−13493